

Point-spread function and MTF characterization of the kinetic-kill-vehicle hardware-in-the loop simulation (KHILS) infrared-laser scene projector

Terri L. Alexander
Glenn D. Boreman
Alfred D. Ducharme

Center for Research in Electro-Optics & Lasers (CREOL)
University of Central Florida, Orlando, Florida 32816

Ronald J. Rapp

Guided Interceptor Technology Branch
Wright Laboratories Armament Directorate
Eglin Air Force Base, Florida 32542

ABSTRACT

A Scophony Infrared Scene Projector (IRSP) is being used at Wright Laboratories Armament Directorate, Guided Interceptor Technology Branch, Eglin AFB, to evaluate thermal-imaging guidance systems. This hardware-in-the-loop testing system reduces the number of necessary field trials and has potential for in-laboratory simulation where the performance of entire seeker systems can be analyzed. The performance of an optical system, in terms of such characteristics as wavefront error, resolution, and transfer factor, can be measured with knowledge of the system MTF and PSF performance. A slow-scan calibration system was used to measure an image plane of the IRSP under three separate configurations of the system. MTFs and PSFs were derived for the IRSP without the use of the scatter screen, with the scatter screen in place, and with the scatter screen rotating.

1. INTRODUCTION

The Kinetic Kill Vehicle Hardware-in-the-Loop Simulation (KHILS) Test Facility is being developed by the Wright Laboratories Armament Directorate, Strategic Defense Division, Guided Interceptor Branch (WL/MNSI), Eglin AFB, FL, to provide nondestructive hardware-in-the-loop performance testing of strategic defense interceptor systems. The main focus of the KHILS system is in performance analysis of seeker systems, signal processing, and guidance, navigation, and control subsystems.¹

Hardware-in-the-loop testing decreases the development time and expense, and has the potential of in-laboratory simulation tests where the performance of entire seeker systems can be analyzed and evaluated with fewer field trials. A major component of the KHILS system is the laser Scophony infrared scene projector (IRSP). A critical element of the IRSP is the scatter screen, which is designed to eliminate laser-coherence effects and to redefine the optical invariant of the projector system to match the unit under test. The infrared scene projector's optical performance and the effects of the scatter screen were investigated.

Fundamental figures of merit for an optical system are its modulation-transfer, optical-transfer, and point-spread functions. This report presents measured data of the IRSP impulse-response intensity profiles with and without the scatter screen. Those data were then used to determine modulation-transfer-function and point-spread-function performance.

2. THEORY

2.1 Laser Scophony IRSP

The KHILS IRSP is a scanned-laser projection system employing Scophony techniques with acousto-optic modulation/deflection devices to project high-resolution 96x96 pixel imagery in a maximum of four infrared wavebands simultaneously. Figure 1 is a diagram of the IRSP optical layout.

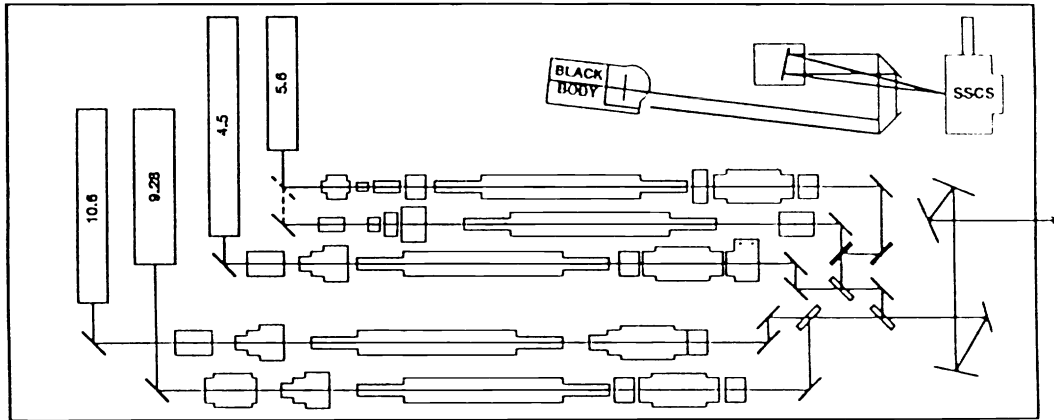


Figure 1. Infrared scene projector optical layout.¹

Scophony modulation uses a collimated laser beam to fill a large portion of the acousto-optic modulator cell. Spreading the laser input allows the projection of multiple pixels simultaneously. This method increases the dwell time of the IRSP on respective seeker/focal-plane-array detectors, which also increases the spatial resolution.^{2,3}

The four laser optical trains can be used in any combination for single- or multiple-wavelength testing. During multi-wavelength operation, the image scan of all optics trains is synchronized, and the outputs are optically combined. Here we focus on the CO₂-laser-driven 9.28- μ m optical train.

A block diagram of the optical system and the Scophony image-scan pattern for a 96x96 pixel format are shown in Fig. 2.

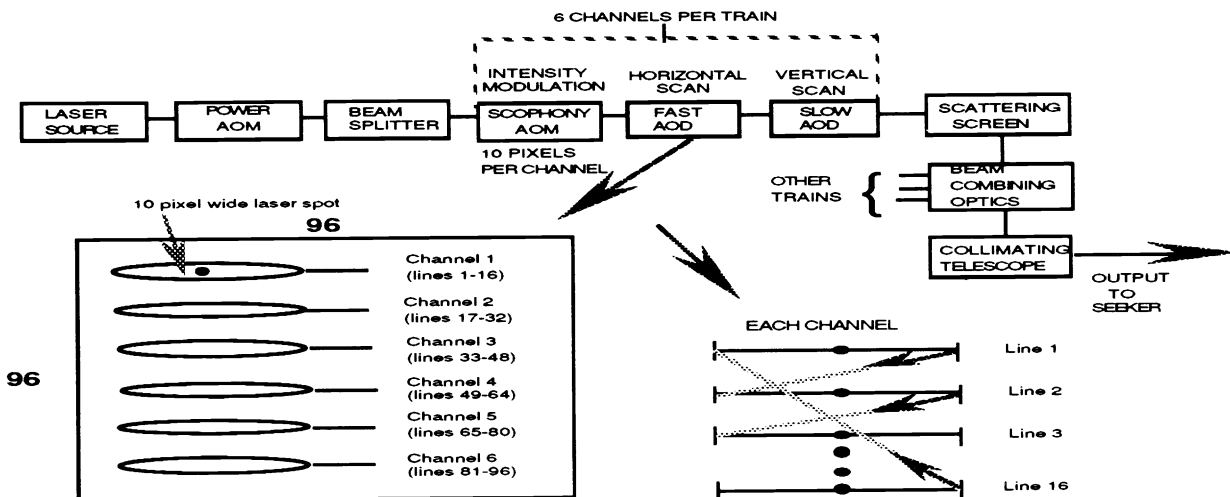


Figure 2. IRSP block diagram and Scophony scan pattern.¹

Active elements in the system include the laser source and the acousto-optic modulator and deflectors (AOMs, AODs). The power AOM is used to attenuate the laser output and control the maximum intensity within the overall image. The beam splitter divides the laser beam into six equal-intensity segments with a 16-line vertical spacing between each segment. The complete 96x96 pixel image is formed using six channels with each channel consisting of 16 lines of 96 pixels each. Within each channel, the Scophony AOM produces a 10-pixel-wide intensity-modulated laser spot, which is scanned over the 96x16 portion of the image using the fast and slow AODs in the pattern shown in the lower portion of Fig. 2. All six channels are scanned simultaneously, so that, at any instant, 60 pixels in the 96x96 image are illuminated.¹

2.2 Scatter screens

The laser sources used in the IRSP produce monochromatic light with high spatial coherence. Although lasers provide an excellent source of high-intensity light, their coherence introduces an interference phenomenon known as laser speckle, which causes a nonuniform intensity pattern. Additionally, as with any optical system, a fundamental characteristic of the IRSP is its optical invariant (lagrange invariant). The optical invariant states that across any surface for a given optical system

$$y_p N u - y N u_p = \text{a constant} , \quad (1)$$

where y_p is the chief ray height, u_p is the chief ray angle with respect to the optical axis, N is the index of refraction, y is the axial ray height, and u is the axial ray angle with respect to the optical axis. A result of this theorem is that if the aperture of a system can be varied, then the angular field must change in inverse ratio to the aperture. The product of aperture height and field angle is constant. Thus increasing one necessitates a reduction of the other.⁴

The scatter screen is a ZnSe circular plate (3 mm thick, 3.8 cm diameter) with an rms roughness of 0.75 μm and anti-reflection coating designed uniquely for use with each wavelength of operation. The scatter screen modifies the optical invariant established at the Scophony acousto-optic modulator, allowing for collimating optics to match the invariant of the seeker. The rms roughness that establishes optimum nonlambertian output without introducing unacceptable attenuation is currently being investigated. In addition to modifying the optical invariant, rotation of the scatter screen causes the beam to encounter different scattering sites and averages out the interference effects. The result is loss of coherence and elimination of laser speckle.⁵

2.3 Point-spread function, optical-transfer function, and modulation-transfer function

A representation of point-spread function, optical-transfer function, and modulation-transfer function relationships their relationships⁶ is shown in Fig. 3.

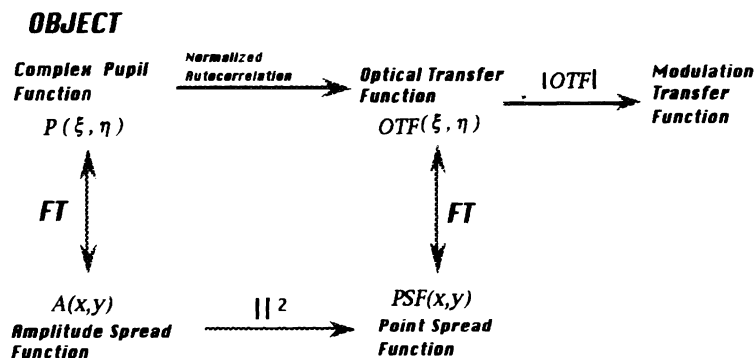


Figure 3. Relationships between different imaging properties of an optical system.

We begin with a complex pupil function $P(\xi,\eta)$ that describes the wavefront shape as it emerges from the IRSP (where ξ and η are the spatial frequencies in the x and y directions). The Fourier transform of $P(\xi,\eta)$ is the amplitude spread function $A(x,y)$, which is a field amplitude and phase. The squared modulus of $A(x,y)$ is the point-spread function $PSF(x,y)$ which is a profile of the resulting irradiance distribution in the image plane. The Fourier transform of the $PSF(x,y)$ is the optical-transfer function $OTF(\xi,\eta)$. The OTF is a measure of an optical system's ability to form high-contrast images. The modulation-transfer function $MTF(\xi,\eta)$ is the modulus of the OTF and is a measure of the reduction in contrast from object to image. If the modulation of a periodic one-dimensional irradiance (I) distribution is defined as

$$\text{modulation depth} = \{I_{\max} - I_{\min}\} / \{I_{\max} + I_{\min}\} , \quad (2)$$

then for a sinusoidal distribution with some spatial frequency ξ , the modulation transfer is the decrease in modulation depth from the object plane to the image plane:

$$\text{modulation transfer} = \text{image modulation} / \text{object modulation} . \quad (3)$$

Plotting the modulation transfer versus spatial frequency is the modulation-transfer function $MTF(\xi)$.⁷

2.4 Measurement methodology

The IRSP output image is projected directly to a seeker under test or folded through a series of mirrors to the slow scan calibration system (SSCS) as shown in Fig. 1. The SSCS has a collimated blackbody source for radiometric and spatial reference. The SSCS uses an off-axis parabola (OAP) with a focal length of 127 cm to focus the IRSP output to an image plane which is scanned by a single-element HgCdTe photovoltaic detector. The resulting irradiance distribution is then used to determine the spatial characteristics of the IRSP image. This arrangement is shown in Fig. 4.

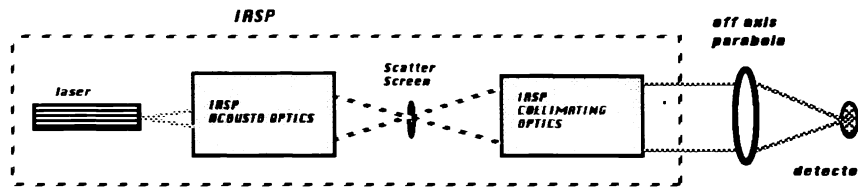


Figure 4. The IRSP output is passed through an off-axis parabola and focused on the detector.

The irradiance data measured by the SSCS are the resultant point-spread functions of the IRSP and the SSCS optical systems. The system measured PSF can be described by the following equation:

$$PSF_{\text{measured}} = PSF_{IRSP} * PSF_{OAP} * w(x) , \quad (4)$$

where $*$ denotes the convolution operator and $w(x)$ is the along-scan width of the detector. The detector contribution to PSF_{measured} is determined by its dimensions. This leaves two unknowns, PSF_{IRSP} and PSF_{OAP} . The contribution of PSF_{OAP} must now be determined.

Measurement of PSF_{OAP} requires consideration of the consequences of source size, detector size, and collimator quality on the measured PSF. The arrangement for determining PSF_{OAP} is shown in Fig. 5.

The scanning detector produces an output voltage $v(x)$ as a function of position. This output voltage is a function of detector width along the scan direction $w(x)$. If the irradiance distribution in the image plane is denoted by $i(x)$ (W/cm^2), the detector output is

$$v(x) = i(x) * w(x) . \quad (5)$$

The irradiance distribution in the image plane $i(x)$ is the convolution of the ideal image with the PSF produced by the collimator/OAP system. The ideal image here is $p(x/dM)$, where $p(x)$ is the pinhole function, d is the diameter of the pinhole, and M is the magnification of the collimator/OAP system. Now we have

$$i(x) = p(x/(dM)) * \text{PSF}_{\text{coll\&OAP}}(x) . \quad (6)$$

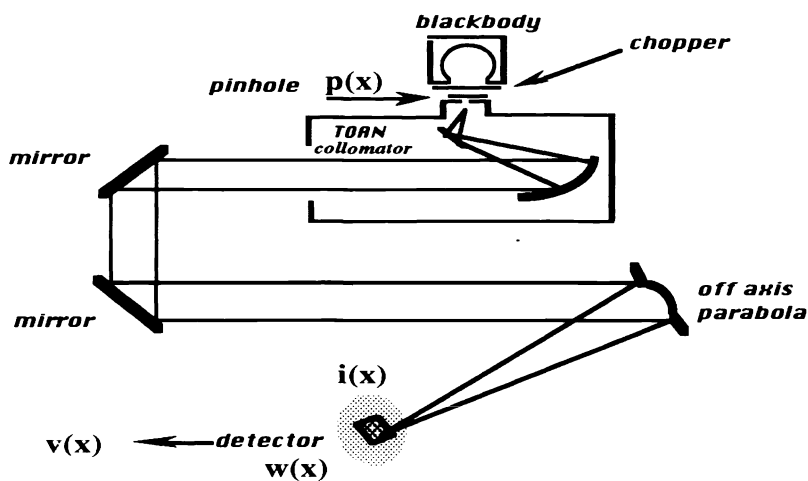


Figure 5. Experimental arrangement for the characterization of the off-axis parabola.

The point-spread function of the collimator and OAP system from Eq. (6) is the convolution of the PSFs caused by aberrations in the collimator and the OAP, as well as the PSF caused by diffraction in the collimator/OAP system. This is

$$\text{PSF}_{\text{coll\&OAP}}(x) = \text{PSF}_{\text{aberr coll}}(x) * \text{PSF}_{\text{aberr OAP}}(x) * \text{PSF}_{\text{diffraction, coll/OAP}}(x) . \quad (7)$$

Assuming the collimator is diffraction limited (this is experimentally verified later), we let $\text{PSF}_{\text{aberr coll}} = \delta(x)$. Using the properties of the convolution with a delta function we now have

$$\text{PSF}_{\text{coll\&OAP}}(x) = \text{PSF}_{\text{aberr OAP}}(x) * \text{PSF}_{\text{diffraction, coll/OAP}}(x) . \quad (8)$$

Diffraction PSF is calculated once for a whole system and is determined by the limiting aperture for the overall optics train. In this case the $\text{PSF}_{\text{diffraction, coll/OAP}}(x)$ is determined by the aperture stop of the collimator and OAP system. Because the OAP is the aperture stop of the system, it will determine $\text{PSF}_{\text{diffraction}}$. This also means that the OAP will be operating at a larger F-number ($F/\#$) than the collimator because the OAP is overfilled by the collimator. However, while this experiment would have the OAP operating at a certain relative aperture determined by the collimator beam overfilling the aperture, once we direct the IRSP into the OAP for characterization of the IRSP, this beam will not overfill the aperture and will cause the OAP to operate at a different $F/\#$. To correct for this, we must know the beam

size generated by the IRSP and apply an aperture stop of equal size directly to the OAP during characterization of the OAP. Therefore, the $PSF_{diffraction\ coll/OAP}$ is $PSF_{diffractionOAP}$. Now

$$PSF_{coll\&OAP}(x) = PSF_{aberr\ OAP}(x) * PSF_{diffraction\ OAP}(x) = PSF_{OAP}(x) . \quad (9)$$

Returning to Eqs. (5) and (6) and making appropriate substitutions, we have an expression for the measured data:

$$v(x) = w(x) * p(x/(dM)) * PSF_{OAP}(x) . \quad (10)$$

In a diffraction-limited system, the point-spread function would correspond in shape to the diffraction pattern produced by a point source. For a small pinhole and a small detector, this would be the case and $v(x)$ would equal PSF_{OAP} . But for a finite detector and a finite pinhole, the effects of this convolution must be considered.

Recall that a convolution in the spatial domain is a multiplication in the Fourier domain.⁸ If we take the Fourier transform of Eq. (10) and divide out the detector and pinhole effects we have the MTF of the OAP:

$$\begin{aligned} V(\xi) &= W(\xi) \times P(\xi M d) \times MTF_{OAP}(\xi) \\ \text{and} \\ MTF_{OAP}(\xi) &= V(\xi) / \{W(\xi) \times P(\xi M d)\} . \end{aligned} \quad (11)$$

Calculation of the PSF of the OAP is performed by inverse Fourier transforming the MTF_{OAP} .

With this accomplished, we direct the IRSP to the detector by way of the OAP as in Fig. 4 and recalling Eq. (4):

$$PSF_{measured} = PSF_{IRSP} * PSF_{OAP} * w(x) . \quad (12)$$

In the Fourier domain:

$$\begin{aligned} MTF_{measured} &= MTF_{IRSP} \times MTF_{OAP} \times W(\xi) , \\ MTF_{IRSP} &= MTF_{measured} / \{MTF_{OAP} \times W(\xi)\} , \end{aligned}$$

and

$$\mathfrak{S}^{-1}\{MTF_{IRSP}\} = PSF_{IRSP} , \quad (13)$$

where \mathfrak{S}^{-1} denotes the inverse Fourier transform.

3. EXPERIMENTAL PROCEDURE

The objective of this experiment was to measure baseline performance of the infrared scene projector for three cases: (1) without the scatter screen; (2) with the scatter screen in place; and (3) with the scatter screen in place and rotating. The measured data were then used to determine point-spread and modulation-transfer functions for all three cases.

An off-axis Newtonian collimator was used during measurements to determine PSF_{OAP} as shown in Fig. 5. Collimation of the output beam was verified with a theodolite and a penta prism.

To ensure that the OAP operates at the same F/# during its characterization as it does during IRSP data collection, IRSP collimated beam size must be determined. The size of the pupil was measured to be 4.6 cm in diameter. A pliable plastic material was fitted to the OAP aperture with a centered opening 4.6 cm in diameter.

During OAP data collection, we used a scanning program written for the SSCS that uses a digital oscilloscope and scans the entire image plane then displays the measured voltages on a CRT. A complete two-dimensional image sample is obtained. With the OAP characterization data we proceed with the IRSP characterization.

Using the arrangement in Fig. 4 and the previously described scanning procedure, measurements were taken over the entire image plane of one pixel for each configuration: without the scatter screen, with the scatter screen, and with the scatter screen rotating. An interactive data language⁹ (Precision Visuals: PV WAVE) was used at a VAX workstation to generate three-dimensional plots of the measured data, MTFs, PSFs, and contour plots of the PSFs for each of the three cases. Calculations were performed manually for a horizontal dimensional analysis of the MTF and PSF of the IRSP without the scatter screen to verify computer results with excellent agreement, and are included in the results section for comparison.

4. RESULTS

4.1 IRSP without the scatter screen

The irradiance distribution of the image plane without the scatter screen is shown in Fig. 6. The projected image is of one pixel, and a Gaussian distribution is expected. Without the scatter screen, the output is circular in the x-y plane but does not appear Gaussian from the perspective of Fig. 6. Although the fluctuations in the peak values rule out any saturation possibilities, there does appear to be an on/off quality. This effect was caused by defocusing attributable to the removal of the scatter screen and the resulting shorter optical path length. The missing scatter screen could also be responsible for a mismatch in F/#s occurring between the acousto-optic subsystem and the collimating optics.

Figure 7 is a plot of the modulation transfer function of the IRSP without the scatter screen. The plot shows two curves of modulation transfer versus frequency in cycles per mm. The solid line represents the modulation transfer in a horizontal slice of the MTF. The dotted line represents the vertical MTF. To obtain the MTF in terms of cycles/mrad these values must be divided by the OAP focal length of 127 cm.

Figures 8 and 9 are plots of the point spread function of the IRSP without the scatter screen. Figure 8 is a three-dimensional plot and Fig. 9 is a contour plot of the PSF as it would look viewed from above. The center represents the maximum value of one, and each line decreases in magnitude by one tenth. Again, to obtain angular spot size, divide linear dimensions by 127 cm. At the half power-points, the angular spot size calculates to approximately 394 μ rad horizontally and 354 μ rad vertically. These results are within expected values.

As a check to the computer-based calculations, the modulation-transfer function and the point-spread function for the IRSP shown in Fig. 10 were calculated manually using Fourier transform tables, division of OAP and detector effects, and inverse-Fourier transformation described in Section 2.4.

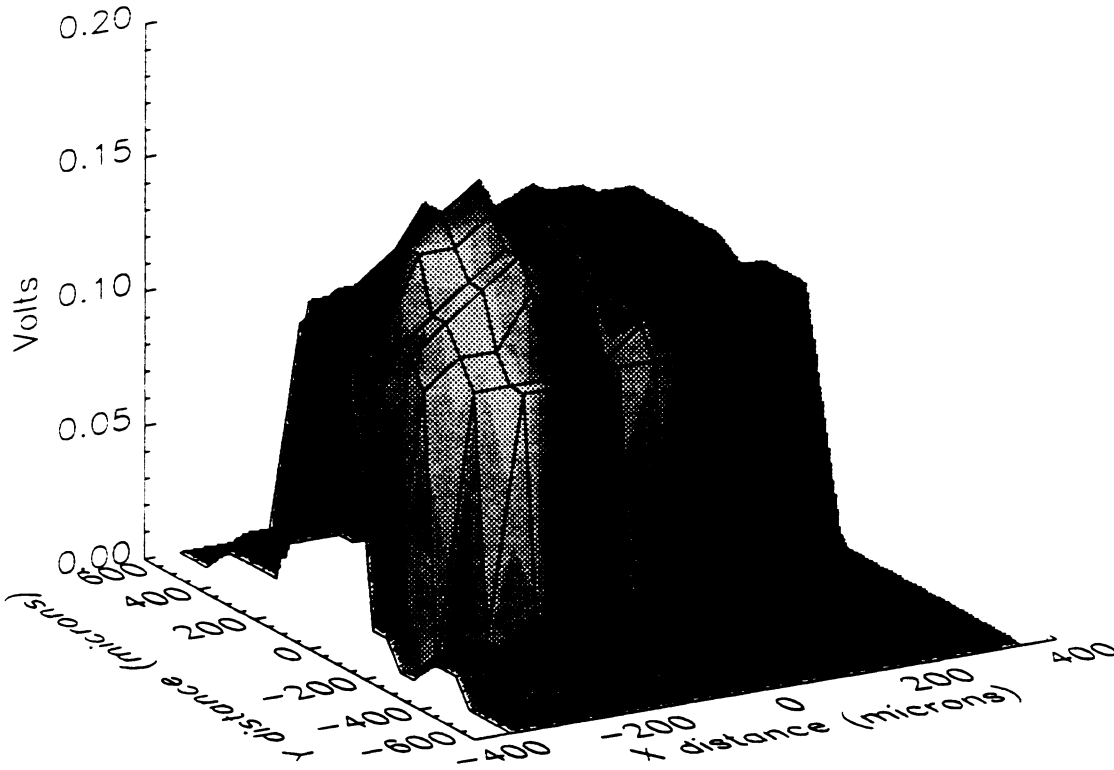


Figure 6. Image-plane irradiance distribution of the IRSP without the scatter screen.

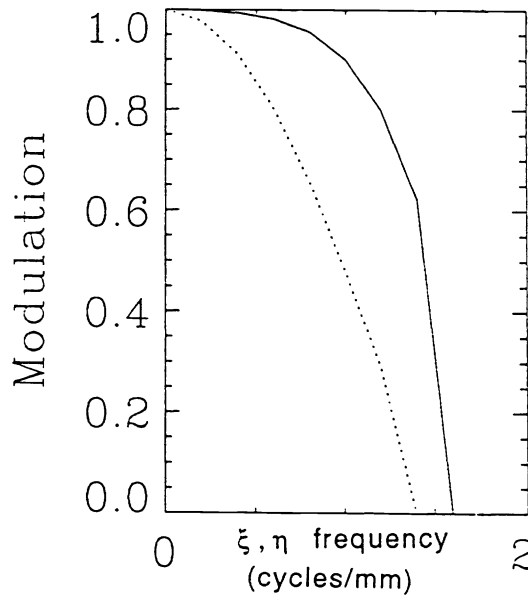


Figure 7. MTF of the IRSP without the scatter screen. The solid line is the horizontal MTF and the dotted line is the vertical MTF in cycles per mm.

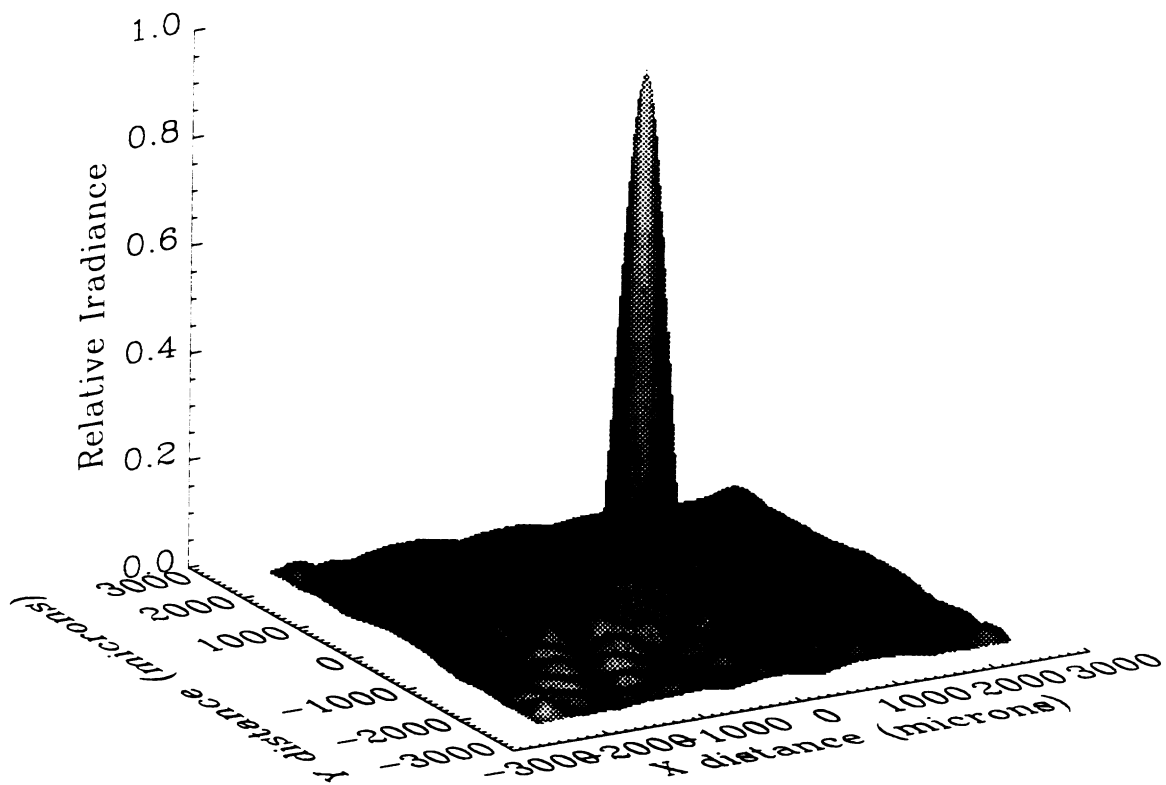


Figure 8. Point-spread function of the IRSP without the scatter screen.

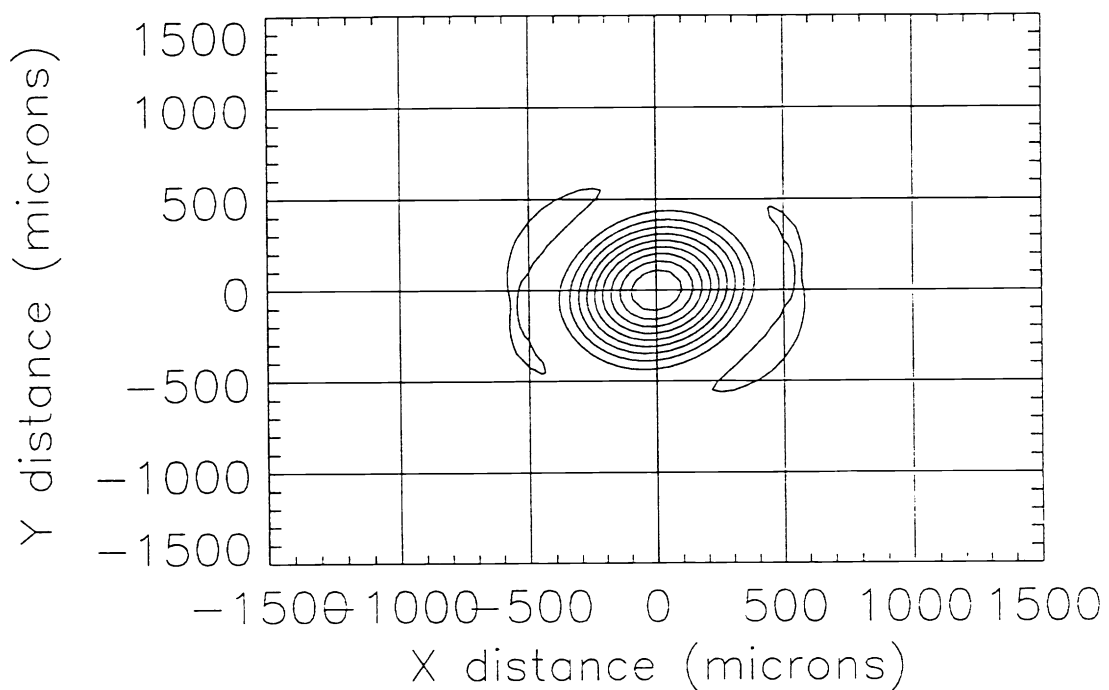


Figure 9. Contour of the IRSP PSF without scatter screen. The center magnitude is one and each level decreases by one tenth.

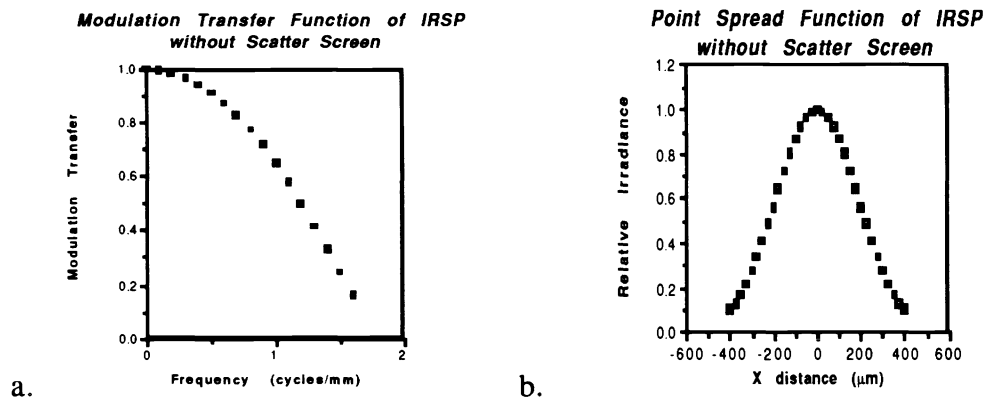


Figure 10 . Manually calculated (a) MTF and (b) PSF of the IRSP without the scatter screen.

Comparison of the manually calculated MTF and the FFT computer-generated MTF shows excellent agreement and, in fact, the actual modulation transfer in the horizontal direction remains stronger at longer frequencies than the calculated MTF. Point-spread functions compare ideally.

4.2 IRSP with the scatter screen

With the scatter screen in place, the measured irradiance distribution is quite smooth, uniform, and Gaussian (Fig. 11). Recall that rotation of the scatter screen destroys laser coherence and eliminates laser speckle. There are no signs of degradation caused by laser speckle without rotation of the screen. It appears that coherence has already been lost by the time the beam reaches the scatter screen, perhaps because of dust and mirror/lens bidirectional reflectance/transmittance distribution function (BRDF/BRTF) scatter. The slightly larger intensity distribution (472 μ rad horizontally) can be attributed to the increasing angle in which energy is distributed after passing through the scatter screen.

Figure 12 is the MTF in the horizontal and vertical direction of the IRSP without the scatter screen. A small decrease in modulation transfer can be expected because of the presence of the scatter screen. Figure 13 is the point-spread function and Fig. 14 is the contour of the PSF of the IRSP with the scatter screen.

4.3 IRSP with the scatter screen rotating

As the scatter screen rotates, the beam strikes a different portion of the screen for each slow-scan sample position and integration time. As the detector scans the region, it collects data at approximately one sample per second. The IRSP is generating frames at 1 per 320 μ s. Each data point is taken at a different frame and pixel dwell time and each sample is at a random position of the scatter screen. This is not the intended configuration for use with the rotating scatter screen. When testing a staring focal-plane array (FPA), individual detectors would see a larger number of scatter sites during an integrating time. An averaging effect similar to what was observed for the static scatter screen with slow-scan detection is expected. The use of the slow-scan calibration system to measure spatial intensity with the scatter screen rotating was thus determined to be invalid. Rotation of the screen also introduces a deviation sight line which results in a larger spot because of a slight wedge angle on the scatter screen. Figure 15 is the MTF in the x and y directions.

Figure 16 is the PSF of the IRSP and Fig. 17 is the contour plot of the PSF with the scatter screen rotating.

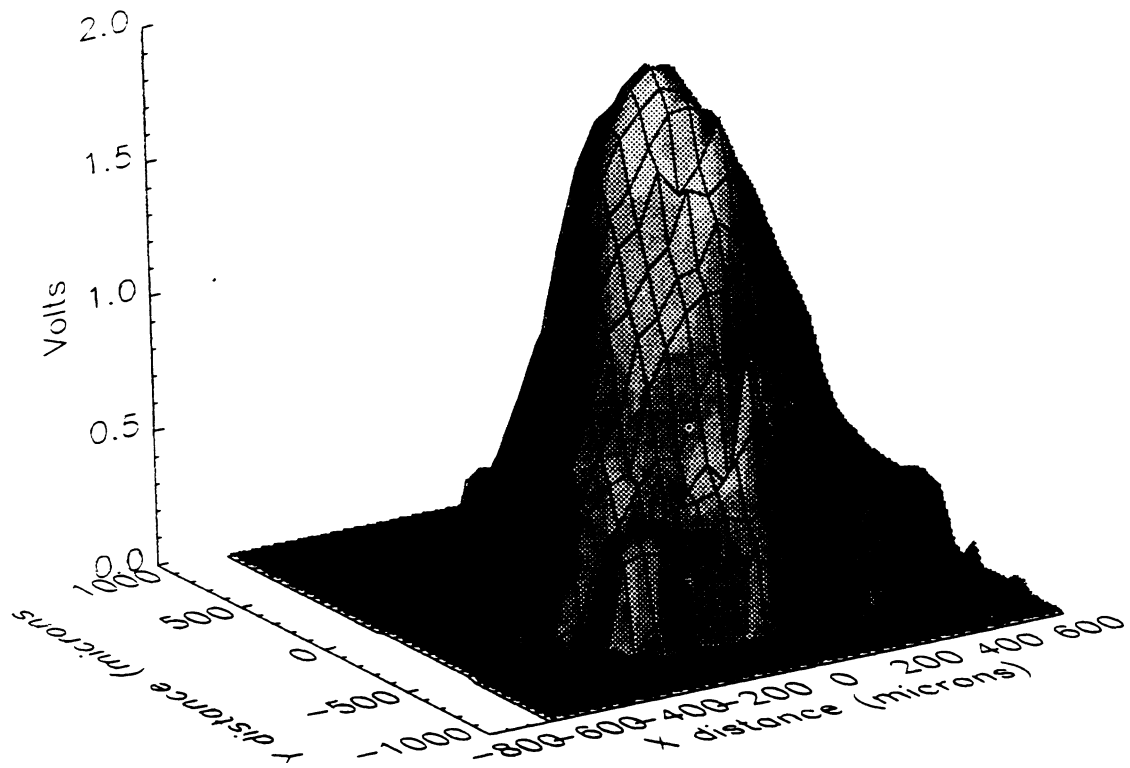


Figure 11. Image-plane irradiance distribution for the IRSP with the scatter screen.

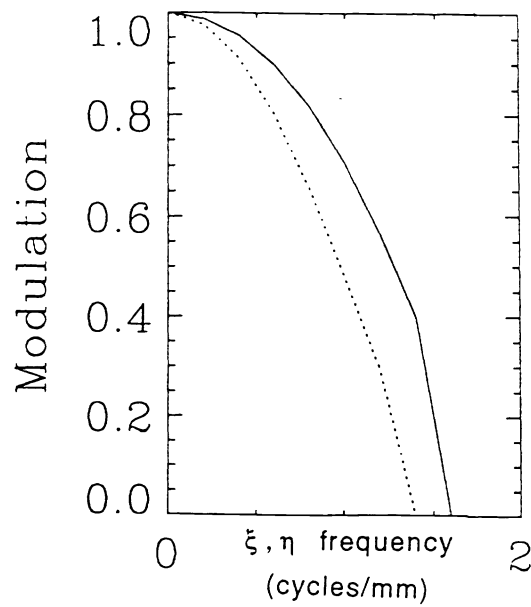


Figure 12. MTF in the x (solid line), and y (dotted line) of the IRSP with scatter screen.

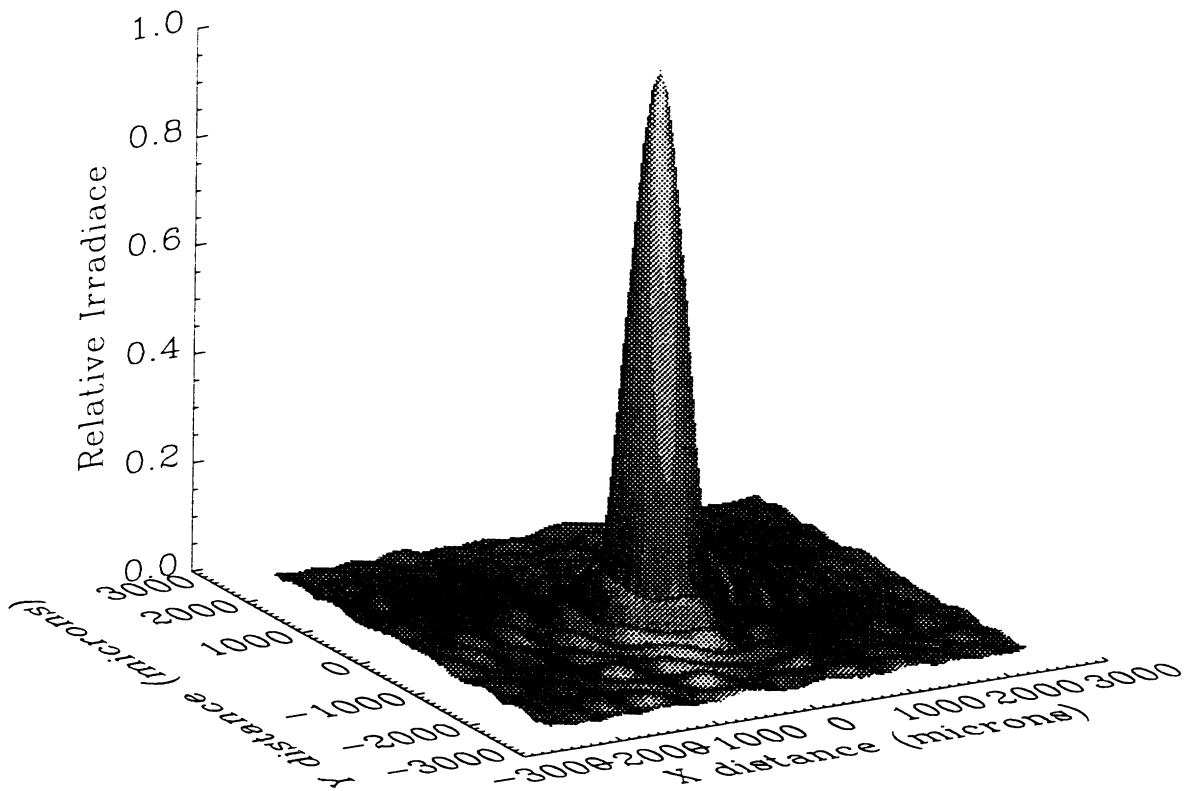


Figure 13. Point-spread function of the IRSP with the scatter screen.

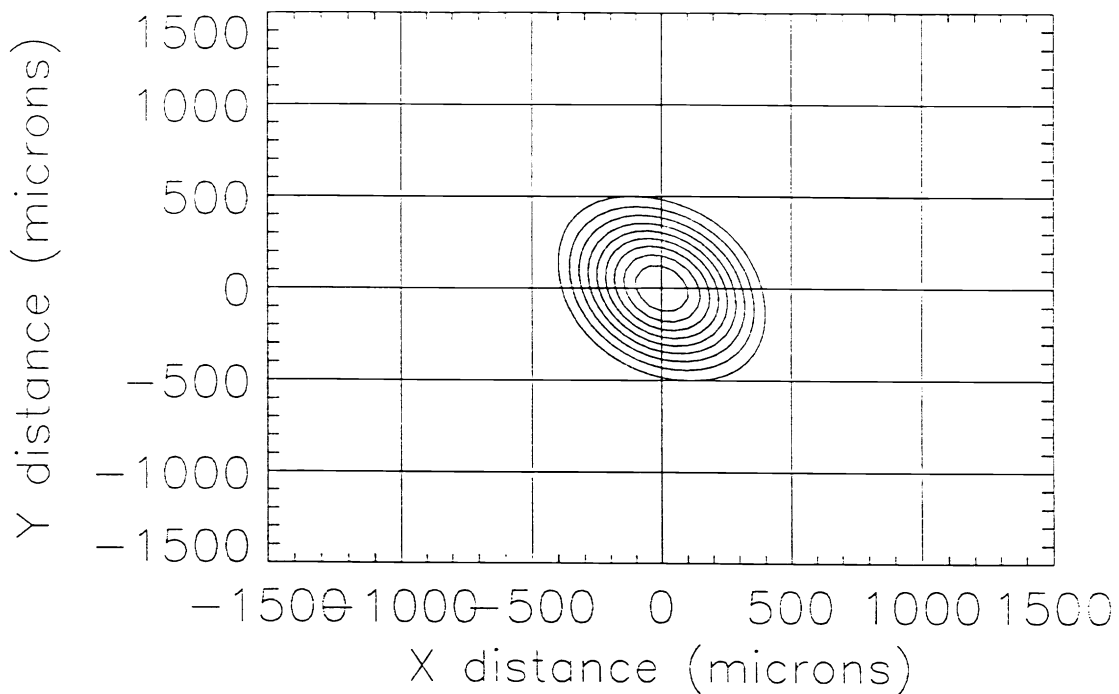


Figure 14. Contour of the IRSP PSF with the scatter screen. The center magnitude is one and each level decreases by one tenth.

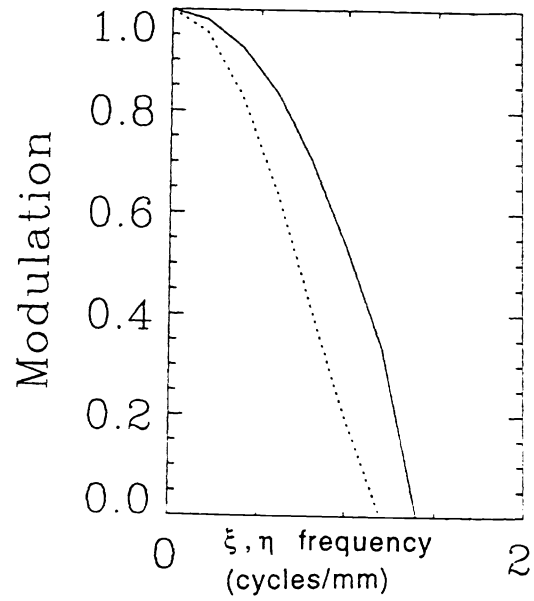


Figure 15. MTF of the IRSP in the x (solid line) and y (dotted line) directions with the scatter screen rotating.

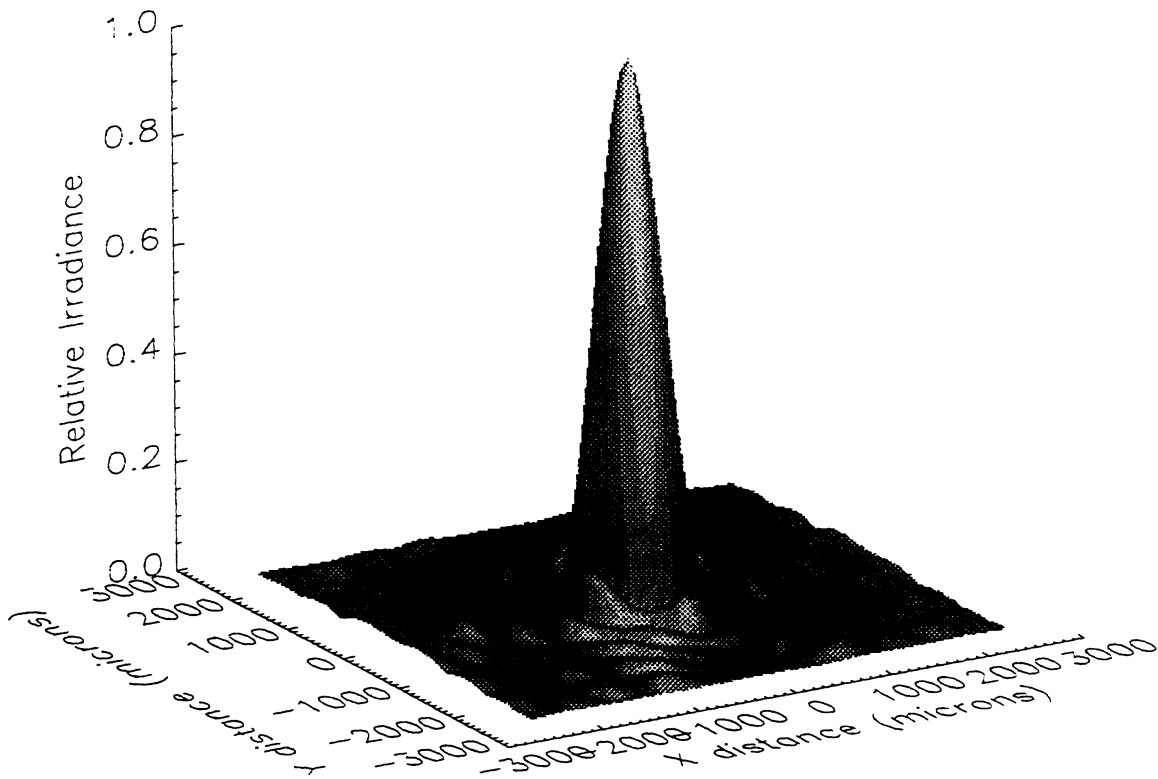


Figure 16. PSF of the IRSP with the scatter screen rotating.

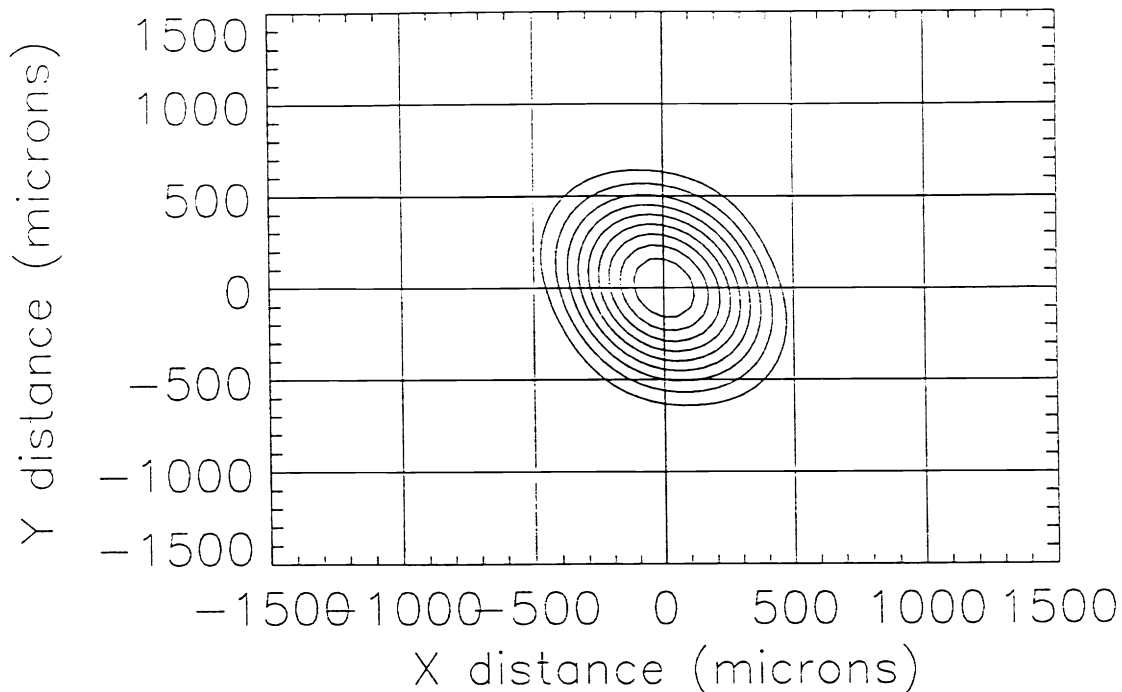


Figure 17. Contour plot of the IRSP PSF with the scatter screen rotating. Center magnitude is one and each level decreases by one tenth.

5. CONCLUSION

The objective of this experiment was to determine the point-spread and modulation-transfer functions of a laser Scophony modulated KHILS infrared scene projector for three separate configurations: (1) without the scatter screen, (2) with the scatter screen in place, and (3) with the scatter screen rotating.

The results are shown in Section 4, where for each configuration we have included plots of 1) the original measured data, 2) an MTF curve in the x and y directions, 3) a three-dimensional plot of the PSF, and 4) a contour plot of the PSF.

The effects of the scatter screen on the measured data, the MTFs, and the PSF, are shown and discussed in the results section. It is shown that a defocusing and mismatch of F/#s possibly occurred while the scatter screen was removed and, although the SSCS scanning stage is mechanized and calibrated to 0.5 μm movements in the x and y directions, there is no similar control for the z direction. Laser-speckle degradation was expected while the scatter screen was not rotating but was not evident in the results explained by BRDF/BRTF scatter. A larger spot size was attributable to the increased angle after passing through the scatter screen. Large fluctuations occurred in the measured image plane while the scatter screen was rotating. This is explained by the slow scan with respect to frame time.

6. ACKNOWLEDGMENTS

Steve Marlow, Bob Richwine and Jim Kircher made significant contributions to this investigation. Their knowledge, experience, and support in the lab made the success of this project possible and it is sincerely appreciated.

This work was supported by the Air Force Office of Scientific Research, Summer Research Program.

7. REFERENCES

1. "KHILS Facility Description and Test Article Interface Document," Guided Interceptor Technology Branch, Wright Laboratories Armament Directorate, Eglin AFB, FL (1991).
2. R. V. Johnson, "Scophony light valve," *Applied Optics*, Vol. 18, No 23, 1 December 1979.
3. E. F. Schildwachter, G. D. Boreman, "Modulation transfer function characterization and modeling of a Scophony infrared scene projector," *Optical Engineering*, Vol. 30, No. 11, November 1991.
4. W. J. Smith, *Modern Optical Engineering*, pg 47, McGraw-Hill, Inc. 1966.
5. R. J. Johnson, "Diffusion and Throughput Measurements of Various Transmissive Screens," *Calspan Corporation/AEDC Operations*. AEDC-TMR-89-V5, March 1989.
6. J. E. Harvey, R. A. Rockwell, "Performance characteristics of phased array and thinned aperture optical telescopes", *Optical Engineering*, Vol. 27, No. 9, pp. 762-768, September 1988.
7. G. D. Boreman, "Transfer Function Techniques," *Handbook of Optics*, Second Edition, McGraw-Hill.
8. J. D. Gaskill, *Linear Systems, Fourier Transforms, and Optics*, John Wiley & Sons, 1978.
9. Precision Visuals: PV WAVE Reference Manual.